INTERNATIONAL JOURNAL OF NOVEL RESEARCH AND DEVELOPMENT (IJNRD)
© 2026 IJNRD | Volume 11, Issue 8, August 2026 | ISSN: 2456-4184 | IJNRD.ORG

Synthesis and Performance Evaluation of a Cellulose–Hydroxyapatite–Graphene Activated Carbon Composite for Groundwater Defluoridation

Bhawna Choudhary[1] and Mangalshree Dulawat[1*]
[1]Department of Chemistry, Janardan Rai Nagar Rajasthan Vidhyapeeth (Deemed to be University), Udaipur Rajasthan, India, 313001.

Abstract:

Excess fluoride in groundwater poses a significant threat to public health in many parts of Rajasthan, particularly in the Dungarpur district, where groundwater serves as the primary source of drinking water. The present study reports the development and evaluation of a sustainable Cellulose–Hydroxyapatite–Graphene Activated Carbon (CHGAC) composite as an efficient adsorbent for groundwater defluoridation. Groundwater samples collected from borewells, open wells, hand pumps, and municipal water supply points were treated using the synthesized composite under optimized adsorption conditions. The CHGAC demonstrated excellent fluoride removal performance, achieving a removal efficiency of approximately 95% during the initial treatment cycle while consistently reducing fluoride concentrations to within acceptable drinking water limits. Regeneration studies confirmed the material's durability, with fluoride removal efficiency remaining above 80% after eight consecutive adsorption–desorption cycles, indicating good structural stability and retention of active adsorption sites. The synergistic interaction of cellulose, hydroxyapatite, graphene, and activated carbon contributes to enhanced adsorption capacity, mechanical stability, and reusability. These findings highlight the potential of CHGAC as an environmentally friendly, cost-effective, and reusable adsorbent for sustainable groundwater treatment, particularly in fluoride-affected rural and semi-arid regions.

Keywords: Cellulose–Hydroxyapatite–Graphene Activated Carbon (CHGAC), Groundwater defluoridation, Fluoride adsorption, Regeneration, Reusable adsorbent, Sustainable water treatment

Introduction:

Groundwater contamination by fluoride has become a major environmental and public health concern due to its widespread occurrence and long-term health implications. Fluoride enters groundwater predominantly through the natural weathering and dissolution of fluoride-bearing minerals such as fluorite, fluorapatite, cryolite, mica, and biotite present in geological formations. The extent of fluoride enrichment depends on several hydrogeochemical factors, including rock composition, groundwater residence time, pH, and climatic conditions, with elevated concentrations frequently observed in arid and semi-arid regions where groundwater is the primary source of drinking water [1,2].

At low concentrations, fluoride plays an important role in maintaining healthy teeth and bones by reducing the incidence of dental caries. However, excessive intake through drinking water can have detrimental effects on human health. To minimize these risks, the World Health Organization (WHO) has established a guideline value of 1.5 mg L^{-1} for fluoride in drinking water. Similarly, the Bureau of Indian Standards (BIS IS 10500:2012, Amendment 2024) recommends a desirable limit of 1.0 mg L^{-1} and a permissible limit of 1.5 mg L^{-1} when no alternative source of safe drinking water is available [3,4].To address this challenge, a range

of defluoridation technologies have been developed and evaluated [5]. Chemical precipitation, coagulation–flocculation, ion exchange, membrane processes including reverse osmosis and nanofiltration, and electrochemical procedures are examples of conventional techniques [6]. Chemical precipitation often utilizes metal salts to form insoluble complexes with fluoride ions, but it typically produces large volumes of sludge requiring safe disposal [7]. Ion exchange resins can selectively remove fluoride; however, they are expensive, exhibit limited selectivity in complex water matrices, and require frequent regeneration [8]. Membrane processes achieve high removal efficiency but demand significant energy input, skilled operation, and recurring maintenance, making them less suitable for decentralized or rural contexts [9]. Electrocoagulation and electrochemical methods offer promising removal efficiencies but suffer from electrode passivation and high operational costs [10]. Because of its low energy requirements, flexibility of design for point-of-use systems, operational simplicity, and adaptability to a variety of water chemistries, adsorption has become one of these methods' most practical and economical options [11].

In recent years, extensive research has focused on developing novel adsorbent and catalytic materials for enhanced fluoride removal. Activated alumina remains a conventional adsorbent because of its high surface area and affinity for fluoride; nonetheless, its effectiveness is strongly pH-dependent, and regeneration is restricted [12]. Iron-, aluminum-, and zirconium-containing oxides and hydroxides have attracted considerable attention for fluoride remediation due to their strong affinity toward fluoride ions through adsorption and exchange processes occurring at the material surface [13]. Biochar and carbonaceous materials derived from agricultural waste have gained interest owing to their sustainability, tunable porosity, and surface functionality [14]. Promising adsorption capabilities and quick kinetics have been shown by nano-structured materials as graphene-based materials, metal-organic frameworks (MOFs), layered double hydroxides (LDHs), and nanohydroxyapatite [15]. Particularly, hydroxyapatite ($Ca_{10}(PO_4)_6(OH)_2$) has shown strong affinity for fluoride through exchange of hydroxyl groups with fluoride, forming fluorapatite, a thermodynamically stable phase [16]. Combining metal oxides with carbonaceous supports has enhanced adsorption efficacy by combining ion exchange, surface complexation, and electrostatic interactions. Graphene oxide and reduced graphene oxide provide large surface area, rich oxygen functional groups, and quick ion transport routes [17]. However, a number of these cutting-edge materials have drawbacks, including difficult synthesis processes, expensive manufacturing costs, restricted regeneration, and decreased suitability in actual water samples with competing ions [18].

To overcome these limitations, there is a pressing need for sustainable, low-cost, and high-performance adsorbents capable of effective fluoride removal under realistic water conditions [19]. Biowaste-derived materials represent an attractive solution due to their renewable nature, low cost, and intrinsic porosity [20]. In this work, we propose the synthesis of a biowaste-derived cellulose–hydroxyapatite–graphene modified activated carbon (CHGAC) using a combination of green and conventional chemical routes [21]. The catalyst integrates the advantages of activated carbon (high surface area), hydroxyapatite (selective ion exchange with fluoride), reduced graphene oxide (enhanced conductivity and rapid adsorption kinetics), and fluoride-affinitive metal sites introduced via surface modification [22]. Cellulose extracted from agricultural waste serves as a structural matrix, improving mechanical stability and facilitating dispersion of active phases. Green synthesis methods using plant extracts (e.g., bael leaf extract) were employed for environmentally benign reduction of graphene oxide. The combined multi-functional approach aims to achieve high adsorption capacity, rapid kinetics, pH resilience, and regenerability, addressing both performance and sustainability metrics. Real groundwater samples were collected from twenty locations with varying fluoride concentrations to evaluate catalyst performance under field-relevant conditions.

In order to provide a scalable solution for sustainable fluoride mitigation in drinking water treatment systems, the main goal of this study is to synthesize, characterize, and assess the fluoride removal efficacy of

the CHGAC using thorough physicochemical analyses, adsorption isotherms and kinetics, and thermal stability assessments.

Result and Discussion:

The morphology of the Biowaste-Derived Cellulose–Hydroxyapatite–Graphene Modified Activated Carbon (CHGAC) was investigated using SEM and (TEM), as shown in **Figure 1**. SEM micrographs at different magnifications **(Figures 1a–c)** reveal a highly porous and interconnected morphology, in which cellulose fibers provide a supportive framework while hydroxyapatite crystals are uniformly dispersed throughout the activated carbon matrix. Distinct rod-like hydroxyapatite particles are observed embedded within wrinkled graphene sheets, contributing to an increased surface area and improved structural stability. The rough and heterogeneous surface morphology confirms the successful incorporation of cellulose, hydroxyapatite, graphene, and activated carbon into a single composite structure.

TEM analysis **(Figure 1d)** further validates the nanoscale distribution of the constituent materials and reveals localized regions of nanoparticle aggregation within the composite. The images provide valuable insight into the internal microstructure, demonstrating the intimate interaction between the different phases of the material. Collectively, the SEM and TEM analyses confirm that the synthesized CHGAC possesses a highly porous architecture with uniformly distributed nanostructures, characteristics that are expected to promote enhanced adsorption efficiency, facilitate mass transfer, and improve the structural stability of the composite during repeated water treatment applications.

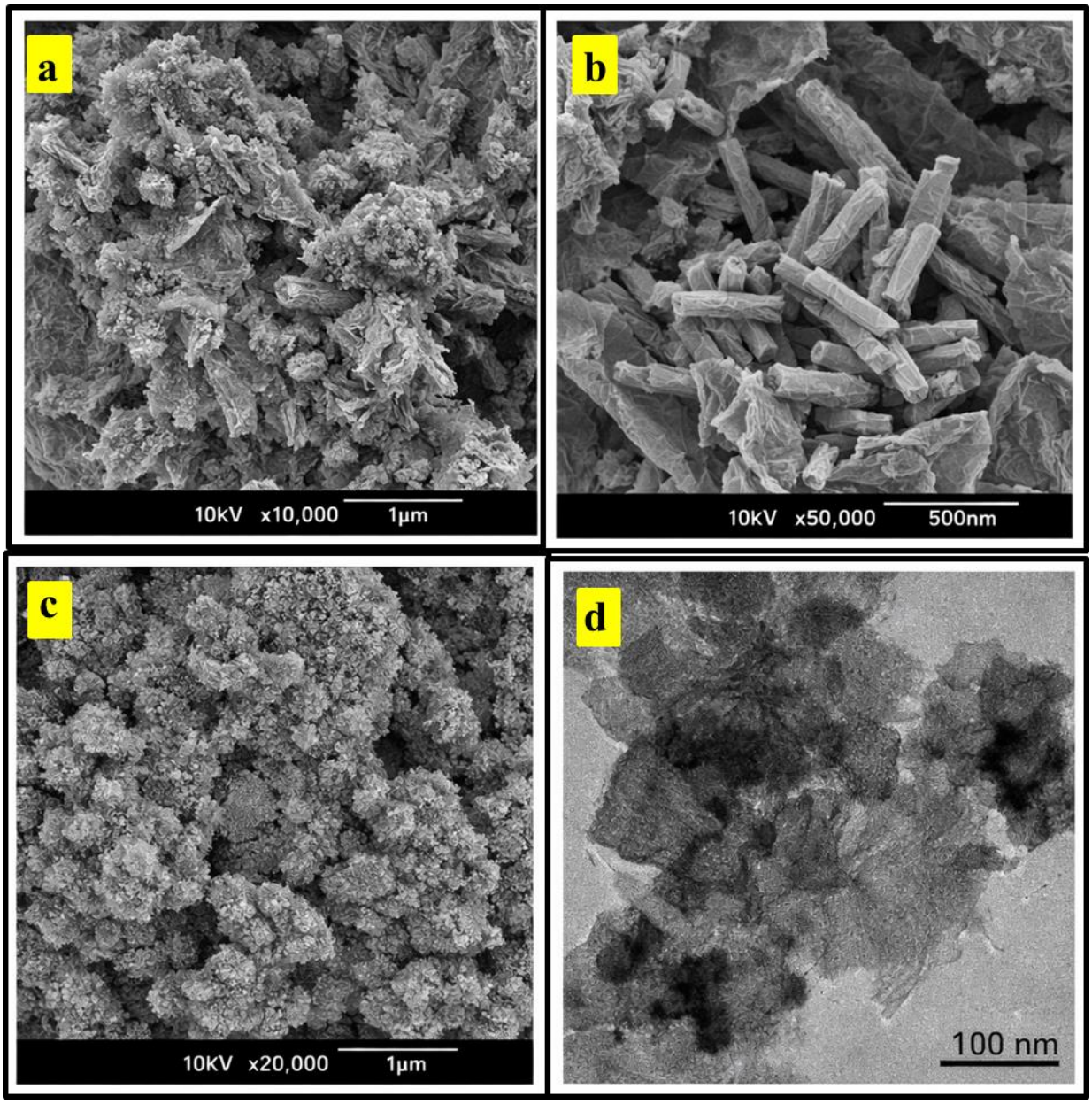

Figure 1: Morphological characterization of the synthesized adsorbent: (a–c) SEM images at different magnifications showing surface texture and particle aggregation, and (d) TEM image revealing internal nanostructure and particle distribution.

The TGA was used to assess the thermal stability of four adsorbent materials: cellulose–hydroxyapatite (CH), graphene oxide (GO), $Al(NO_3)_2$-modified carbon, and the synthesized cellulose–hydroxyapatite–graphene modified activated carbon (CHGAC) catalyst. Mass retention (%) was plotted as a function of temperature over the range of 100–800 °C (Figure 2). The mass of $Al(NO_3)_2$-modified carbon decreased significantly as the temperature rose, from 100% at 100°C to around 45% at 800°C, indicating rather low thermal stabilityGraphene oxide, on the other hand, showed modest thermal stability, keeping around 47% of its initial mass at 800°C. A notable mass loss was noted between 200 and 400°C, which is consistent with the breakdown of functional groups that contain oxygen. By retaining around 55% of its mass at 800°C, the cellulose-hydroxyapatite showed improved heat resistance. The addition of hydroxyapatite, which probably provides structural support and prevents the cellulose matrix from degrading, is credited with this enhancement. Among the materials studied, the synthesized CHGAC catalyst showed the best thermal stability, holding onto around 57% of its mass at 800°C. A strong structural structure that can tolerate high temperatures is suggested by the progressive mass loss seen across the whole temperature range. Together, the TGA findings show that the produced CHGAC catalyst has the best thermal resilience, followed by

graphene oxide, cellulose-hydroxyapatite, and $Al(NO_3)_2$-modified carbon. Because thermal stability directly affects material performance and operational longevity, these facts are crucial for the logical selection of adsorbents and catalysts meant for applications requiring extreme temperatures.

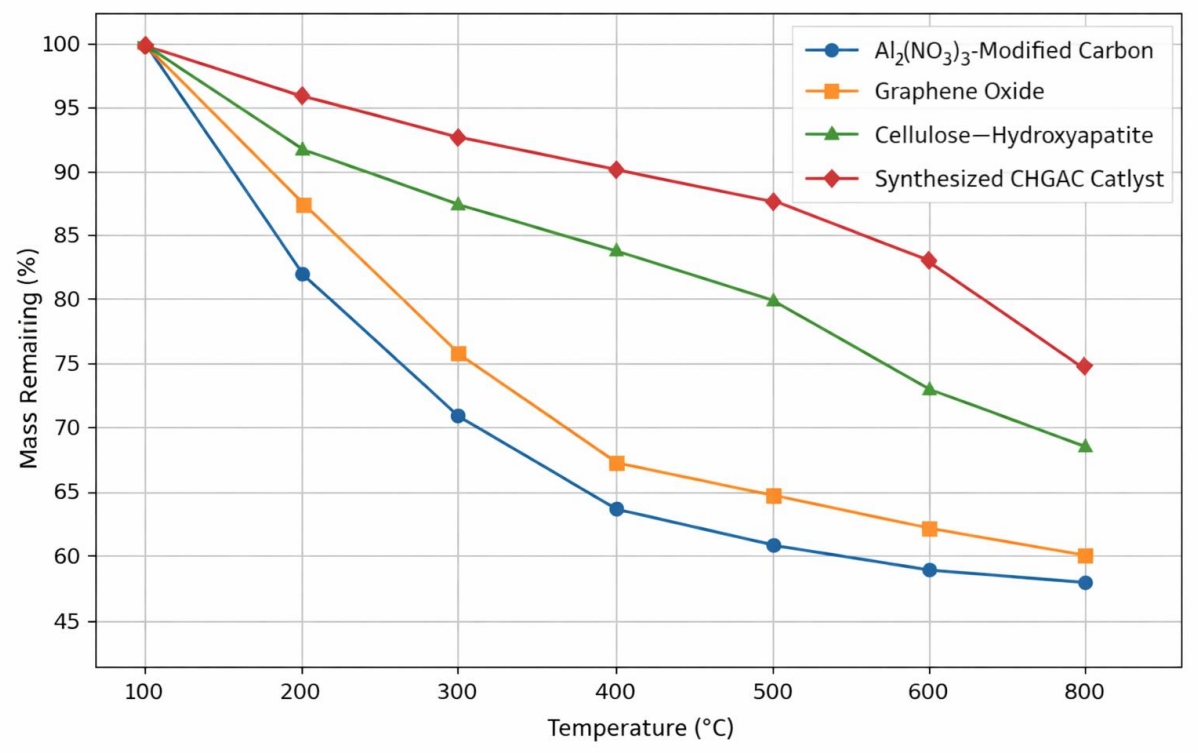

Figure 2: Thermal stability analysis showing mass remaining (%) as a function of temperature for different materials.

To examine their surface chemistry and confirm that the constituent materials were successfully incorporated, the FTIR spectra of $Al_2(NO_3)_3$-modified carbon, graphene oxide (GO), cellulose–hydroxyapatite (Cell–HAp), and the synthesized CHGAC were recorded throughout the range of 4000–500 cm^{-1}. The wide absorption signature about 3350 cm^{-1} in the spectra of $Al_2(NO_3)_3$-modified carbon was attributed to O–H stretching vibrations, whereas the signal near 1611 cm^{-1} was caused by aromatic C=C stretching and/or the bending mode of adsorbed water molecules. The successful integration of aluminum nitrate onto the carbon surface was confirmed by a clear band at around 1385 cm^{-1} that belonged to nitrate (NO_3^-) species.

In the case of graphene oxide, there was a noticeable absorption around 1707 cm^{-1} due to carbonyl (C=O) groups, along with a wide O–H stretching vibration at about 3325 cm^{-1}. The band near 1386 cm^{-1} was attributed to C–O stretching vibrations, which reflects GO's strong oxygenated functioning. Because of the hydroxyl groups, the Cell–HAp composite showed a broad absorption band between 3310 and 3350 cm^{-1}. Another characteristic at 1638 cm^{-1} was linked to bound water molecules and vibrations related to cellulose. The existence of hydroxyapatite in the matrix was confirmed by the strong absorption centered about 1030 cm^{-1}, which was typical of phosphate (PO_4^{3-}) stretching modes. CHGAC's FTIR spectrum included the distinctive characteristics of each of its constituent parts. The absorption at 1094 cm^{-1} was associated with phosphate stretching vibrations, while a wide hydroxyl-related band was seen at about 3328 cm^{-1}. The spectrum study as a whole demonstrated that CHGAC contains hydroxyl, phosphate, nitrate, and oxygen-containing functions. It is anticipated that the quantity of these active surface sites would increase its affinity for fluoride ions, which will improve its adsorption efficiency. **(Figure 3)**

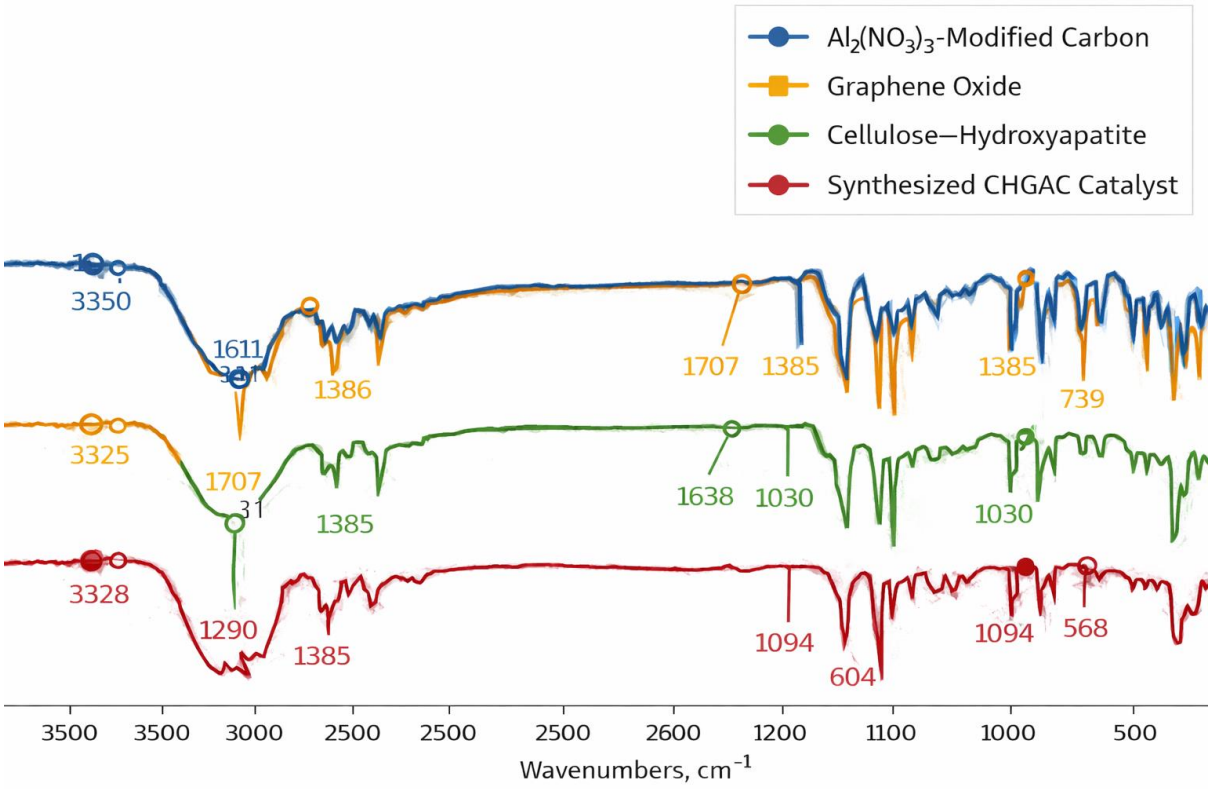

Figure 3: FTIR spectra of different materials showing functional groups at various wavenumbers.

The comparative XRD patterns of $Al_2(NO_3)_3$-modified activated carbon, graphene oxide (GO), cellulose–hydroxyapatite (Cell–HAp), and the synthesized Cellulose–Hydroxyapatite–Graphene Modified Activated Carbon (CHGAC) are presented in **Figure 4**, confirming the structural characteristics of the individual components and the successful formation of the composite. The XRD pattern of $Al_2(NO_3)_3$-modified activated carbon exhibits a broad diffraction hump centered at $2\theta = 20–25°$, characteristic of predominantly amorphous carbonaceous materials. In contrast, graphene oxide shows a prominent diffraction peak at $2\theta \approx 11–12°$, corresponding to the (001) crystal plane, which indicates the oxidation of graphite and the expansion of the interlayer spacing.

The Cell–HAp composite displays well-defined diffraction peaks at $2\theta \approx 25.9°$, 31.8°, 32.9°, 39.9°, and 46.7°**,** which are in good agreement with the characteristic reflections of hexagonal hydroxyapatite (JCPDS No. 09-0432), confirming the successful incorporation of hydroxyapatite into the cellulose matrix. The XRD pattern of the synthesized CHGAC exhibits the combined structural features of its constituent materials, with a noticeable reduction in the intensity of the GO diffraction peak and the presence of distinct hydroxyapatite reflections. These observations indicate the effective incorporation of graphene oxide within the composite and its partial exfoliation during synthesis. Furthermore, the slight broadening of the diffraction peaks suggests a reduction in crystallite size and enhanced interfacial interactions among the composite components. Overall, the XRD analysis confirms the successful synthesis of a structurally stable, semi-crystalline CHGAC composite with characteristics that are expected to favour efficient fluoride adsorption.

Groundwater samples were gathered from several sites within the research region in order to assess the synthesized catalyst's practical suitability for fluoride detection. Twenty water samples (B.C.-1 to B.C.-20) from different settlements and habitations were collected from open wells, tubewells, and hand pumps. After being gathered in sterile plastic bottles, the samples were brought to the lab for examination. Standard techniques were used to measure physicochemical parameters such as alkalinity, nitrate, chloride, total dissolved solids (TDS), magnesium hardness, pH, and fluoride content. Spatial variation in fluoride contamination was shown by the fact that the fluoride content in the collected samples varied substantially

between sites, ranging from sub-permissible to above-permissible levels. The fluoride detection capability of the synthesized CHGAC catalyst under real-world field settings was next evaluated using these genuine groundwater samples. **(Figure 4)**

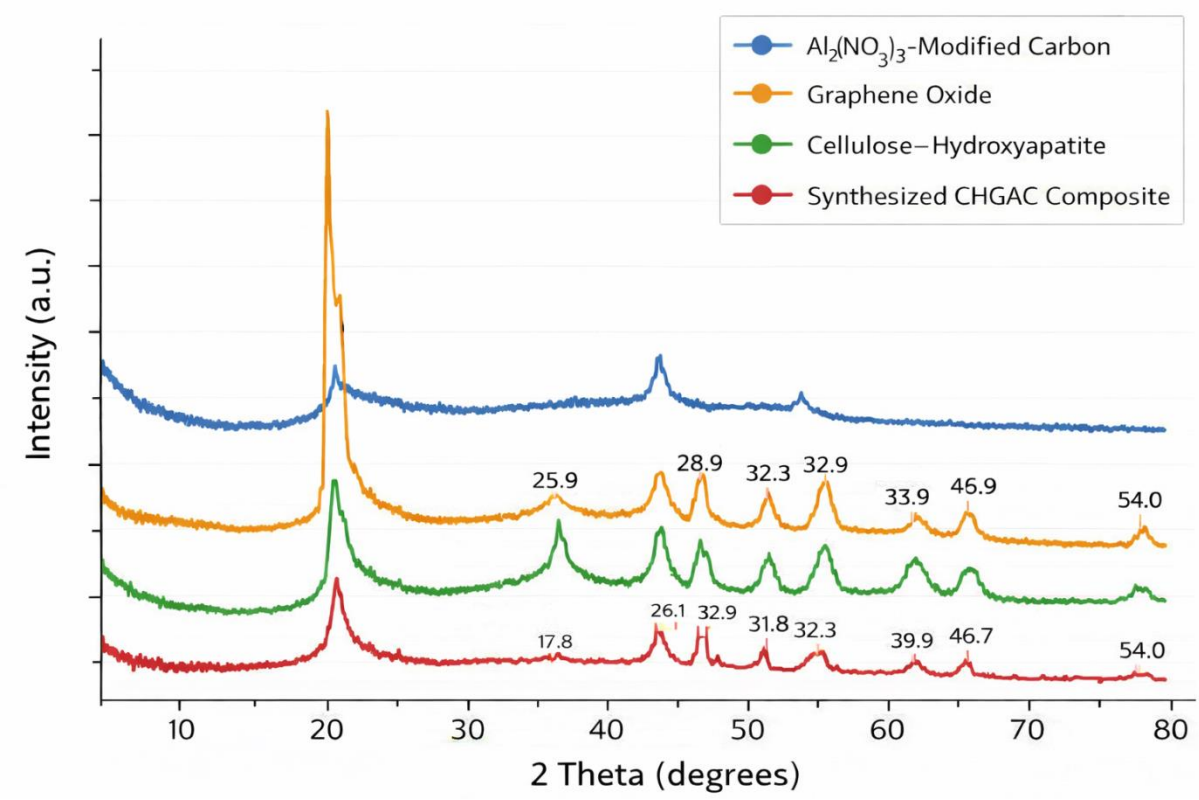

Figure 4: XRD patterns of different materials showing crystallographic structure and phase composition.

Location of the site and geographical of study area : -

The Dungarpur district, which has an area of around 3,770 km², is located in the southern region of the Indian state of Rajasthan. Geographically, it is between latitudes 23°19′42.87′–24°0′42.68′ N and longitudes 73°20′59.23′–74°23′42.87′ E. The district is a part of the Mewar Rocky Region, which is connected to the southern Aravalli hill chain, and the Mahi (Chappan) Basin. Significant topographic variety characterizes its topography, with the northern and western regions being dominated by rough and divided hilly terrain. While reasonably flat plains are more prevalent in the eastern part, pediplains with isolated hillocks and rocky outcrops make up the majority of the remaining area. Dungarpur has an average annual rainfall of around 76 cm and is located in the Humid Southern Plain agroclimatic zone.

The district was home to over 1.38 million people in the 2011 Indian Census; by 2023, that number is predicted to rise to almost 1.61 million. Administratively, Dungarpur is made up of four urban centers like Dungarpur, Sagwara, Galiakot, and Simalwara, as well as nine tehsils and 976 villages. Dungarpur City is the main urban settlement among them. The district still has a number of socioeconomic and developmental challenges, and the majority of its residents are indigenous. With a sizable section of the labor force working in agriculture and cultivation, agriculture continues to be the major driver of the local economy. The district was among Rajasthan's less developed districts in 2011, with a labor participation percentage of 46.2% and a literacy rate of 59.46%.

The need for dependable supplies of drinkable water has increased due to population pressure, urban growth, and industrial development, underscoring the need for efficient water quality evaluation and treatment

methods. The need for wastewater reclamation and the scarcity of freshwater supplies have become significant environmental issues in many areas. Numerous pollutants, such as organic compounds, industrial dyes, solvents, heavy metals, and other potentially dangerous elements that endanger human health and the environment, are frequently found in wastewater streams. Fluoride (F^-) is one of the many contaminants found in water supplies, and its persistence and broad occurrence make it a serious problem. The weathering and dissolution of fluoride-bearing minerals including fluorapatite, cryolite, and villiaumite allows fluoride to infiltrate groundwater systems; human additions come from the use of fertilizers and other industrial processes, such as the production of glass and ceramics. Long-term exposure to high fluoride levels can be harmful to human health, even if fluoride at regulated doses helps maintain dental health by preventing tooth decay. Dental and skeletal fluorosis, renal failure, thyroid problems, bone weakness, and neurological issues have all been linked to excessive fluoride use. Guidelines for fluoride concentrations in drinking water have been set by a number of regulatory bodies to protect public health. Organizations like the American Dental Association and the U.S. Environmental Protection Agency (EPA) advise keeping fluoride levels within a healthy range while establishing higher acceptable limits to reduce harmful health effects. However, studies show that almost 200 million people in more than 25 nations are still at risk of excessive fluoride exposure from drinking water sources, making fluoride pollution a persistent global problem. **(Figure 5)**

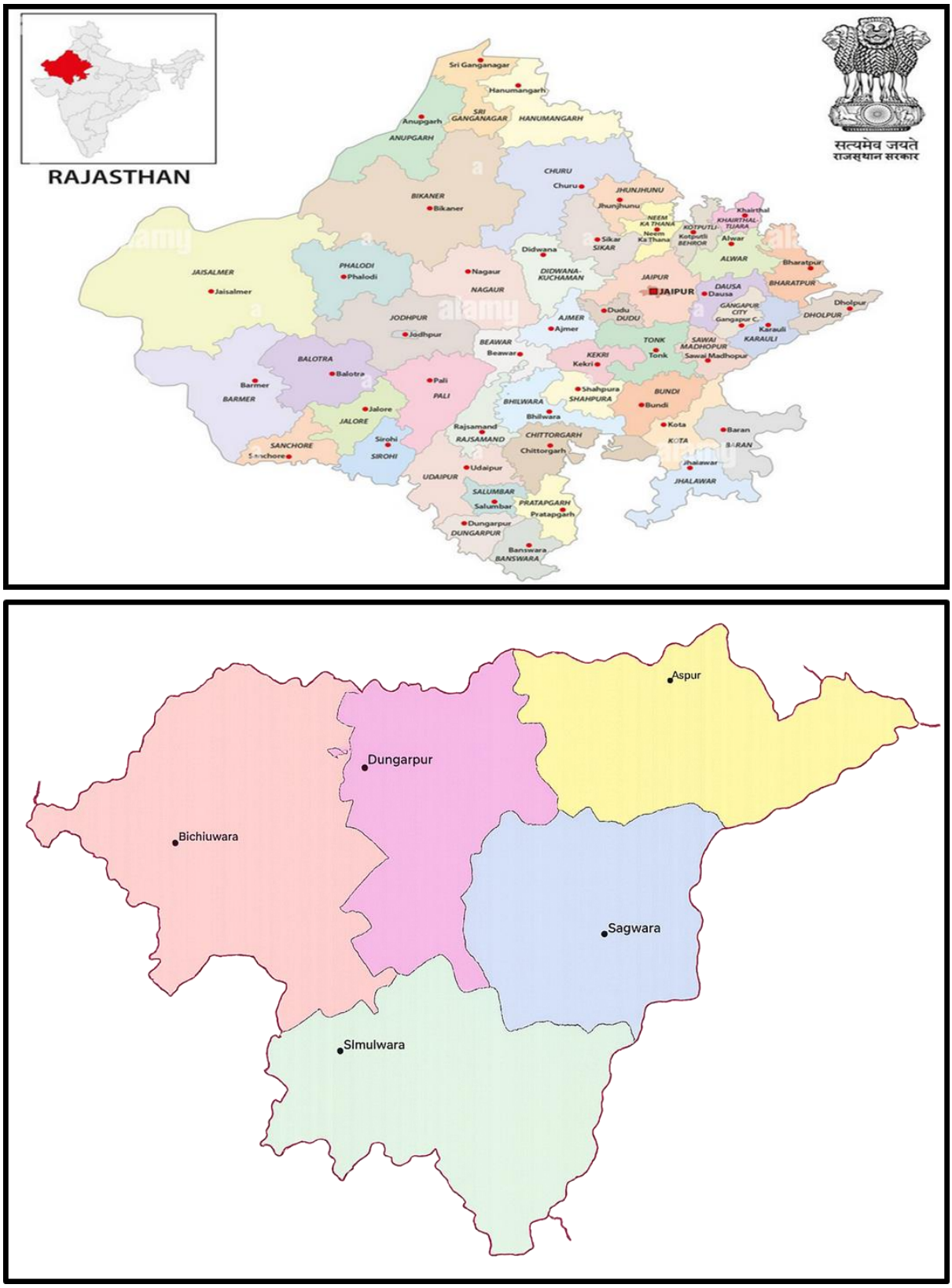

Figure 5: Location map of study area - Aspur

To evaluate fluoride contamination levels and the effectiveness of the synthesized catalyst, water samples were taken from a variety of sources, including groundwater wells, boreholes, hand pumps, and municipal tap water. To avoid changing the fluoride content, each sample was gathered in sterile, previously cleaned polyethylene bottles, kept at 4°C, and examined right away. In order to ensure that the dataset accurately reflects the variety in fluoride levels seen in the actual world, sampling locations were selected to reflect a range of hydrogeological circumstances. Adsorption studies were conducted using the gathered samples to assess the catalyst's performance in various water matrices.

Table 1: Physiochemical analysis of water samples showing mineral contamination in Aspur region.

S.n.	Sample ID	Water Sample	Habitation	Alkalinity (mg/L)	Chloride (mg/L)	Nitrate (mg/L)	TDS (mg/L)	Mg Hardness (mg/L)	Fluoride (mg/L)	pH
1	B.C.-1	Handpump	Kherda	280	378	15	819	1020	3.40	7.40
2	B.C.-2	Handpump	Sundari	326	149	27	878	340	3.50	7.90
3	B.C.-3	Handpump	Kadeliya	280	287	60	773	352	2.80	7.80
4	B.C.-4	Handpump	Moti Dhani	180	159	40	700	450	1.80	7.60
5	B.C.-5	Handpump	Lohera	236	150	45	550	440	3.95	7.40
6	B.C.-6	Handpump	Undva	310	150	22	768	269	0.94	7.60
7	B.C.-7	Handpump	Gopalpura	232	128	29	686	342	1.10	7.58
8	B.C.-8	Tubewell	Kotar	300	142	30	820	240	1.60	7.83
9	B.C.-9	Tubewell	Hamela	222	355	21	698	319	1.75	7.69
10	B.C.-10	Tubewell	Upla Fala	248	388	10	450	746	1.80	7.89
11	B.C.-11	Tubewell	Navan Fala	160	396	9	1012	698	1.20	7.65
12	B.C.-12	Tubewell	Gada	278	146	12	745	420	4.20	7.85
13	B.C.-13	Tubewell	Kadmal Fala	340	350	20	1052	860	0.96	7.28
14	B.C.-14	Tubewell	Vanka	390	250	38	1062	580	1.90	7.49
15	B.C.-15	Openwell	Sandan	270	119	40	794	392	4.10	7.57
16	B.C.-16	Openwell	Karanjiya	32	240	15	1056	330	3.70	7.47
17	B.C.-17	Openwell	Badkota	148	30	47	898	430	1.60	8.15
18	B.C.-18	Openwell	Kundla	252	220	11	667	320	1.80	8.10
19	B.C.-19	Openwell	Mor	342	187	22	687	440	1.85	7.99
20	B.C.-20	Openwell	Badoda	367	153	29	497	490	1.50	7.98

The B.C. adsorbent's field performance for removing fluoride from several groundwater sources (handpump, tubewell, and openwell) throughout many habitations is summarized in the table. After treatment, the initial fluoride concentrations, which varied from 0.94 to 4.20 mg L^{-1}, were successfully lowered to 0.21–0.61 mg L-1. The fluoride removal effectiveness ranged from 76.0% to 85.9%, with samples with higher baseline fluoride levels consistently showing better removal (>80%). The resulting fluoride concentration was consistently below the WHO allowed limit, indicating the adsorbent's resilience and applicability for groundwater defluoridation applications in real-world settings.

Table 2: Effect of composite absorbent on fluoride concentration in water samples.

S. No.	Sample ID	Water Source	Habitation	Initial Fluoride (mg/L)	Final Fluoride (mg/L)	Fluoride Removal (%)
1	B.C.-1	Handpump	Kherda	3.40	0.48	85.9
2	B.C.-2	Handpump	Sundari	3.50	0.52	85.1
3	B.C.-3	Handpump	Kadeliya	2.80	0.45	83.9
4	B.C.-4	Handpump	Moti Dhani	1.80	0.32	82.2
5	B.C.-5	Handpump	Lohera	3.95	0.58	85.3
6	B.C.-6	Handpump	Undva	0.94	0.21	77.7
7	B.C.-7	Handpump	Gopalpura	1.10	0.26	76.4
8	B.C.-8	Tubewell	Kotar	1.60	0.30	81.3
9	B.C.-9	Tubewell	Hamela	1.75	0.33	81.1
10	B.C.-10	Tubewell	Upla Fala	1.80	0.35	80.6
11	B.C.-11	Tubewell	Navan Fala	1.20	0.27	77.5
12	B.C.-12	Tubewell	Gada	4.20	0.61	85.5
13	B.C.-13	Tubewell	Kadmal Fala	0.96	0.23	76.0
14	B.C.-14	Tubewell	Vanka	1.90	0.36	81.1
15	B.C.-15	Openwell	Sandan	4.10	0.60	85.4

16	B.C.-16	Openwell	Karanjiya	3.70	0.55	85.1
17	B.C.-17	Openwell	Badkota	1.60	0.29	81.9
18	B.C.-18	Openwell	Kundla	1.80	0.34	81.1
19	B.C.-19	Openwell	Mor	1.85	0.35	81.1
20	B.C.-20	Openwell	Badoda	1.50	0.28	81.3

Recyclability of CHGAC:

The reusability of the synthesized catalyst was evaluated through repeated adsorption–desorption cycles. After fluoride adsorption, the spent catalyst was regenerated using a mild alkaline washing (e.g., NaOH solution), followed by rinsing and drying. The catalyst retained a high fluoride removal efficiency over multiple cycles, with only a marginal decline observed after successive uses. This indicates that the active adsorption sites remain largely intact and confirms the good recyclability and practical applicability of the catalyst for repeated groundwater defluoridation. **(Figure 6)**

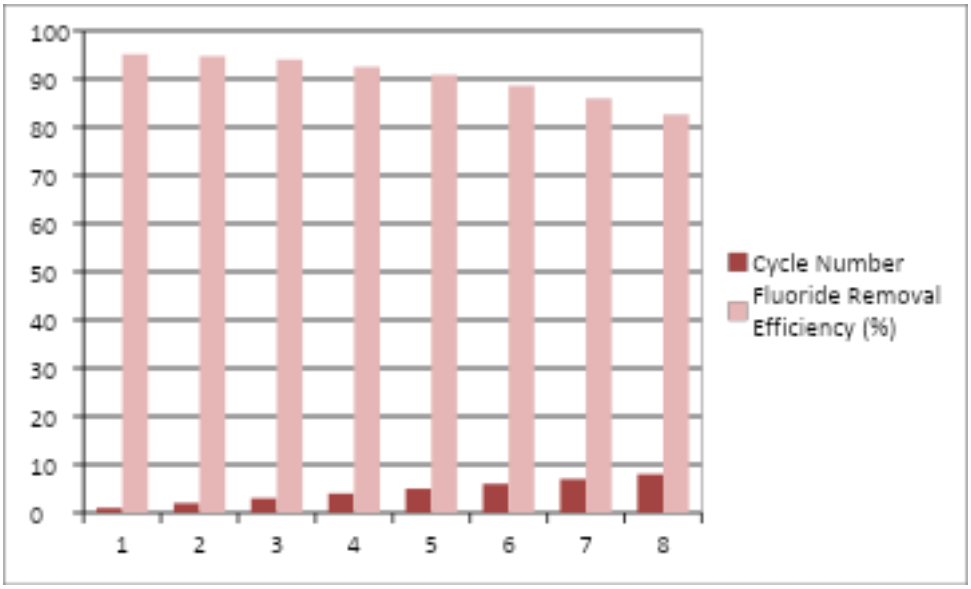

Figure 6: Regeneration and reusability performance of the synthesized adsorbent evaluated through successive adsorption cycles.

Experimental:

General procedure for the synthesis of a Biowaste-Derived Cellulose–Hydroxyapatite–Graphene Modified Activated Carbon (CHGAC)

Step 1: Preparation of Activated Carbon

To create char, biowaste materials like rice husk or coconut shell were completely cleaned with distilled water, oven-dried at 105 °C, then carbonized at 450 °C for two hours with little oxygen. 30 mL of 1 M KOH solution (1:3 w/v) was used to chemically activate the char (10 g), which was then repeatedly cleaned with distilled water until the pH was neutral and dried at 100 °C.

Step 2: Metal Surface Modification

For four hours at room temperature, 5 g of activated carbon was impregnated in 100 mL of 0.1 M $Al(NO_3)_3$ or $MgCl_2$ solution while being continuously stirred. To add fluoride-affinitive metal sites, the mixture was then filtered and dried at 150 °C.

Step 3: Green Reduction of Graphene Oxide

Ultrasonication was used for 30 minutes to disperse 0.2 g of graphene oxide in 200 mL of distilled water. After adding 20 mL of Bael leaf extract, the mixture was heated to 80 °C for two hours to produce reduced

graphene oxide. This was then combined with the metal-modified activated carbon and ultrasonically heated for thirty minutes.

Step 4: Synthesis of Cellulose–Hydroxyapatite

Cellulose fibers (2 g) were dispersed in 200 mL distilled water under stirring. Calcium solution was prepared by dissolving calcined eggshells (3 g) in dilute acetic acid and added dropwise to the cellulose dispersion, followed by slow addition of 0.3 M KH_2PO_4 under alkaline conditions (pH ≈ 10) to allow in-situ precipitation of hydroxyapatite on the cellulose matrix.

Step 5: Assembly of Hybrid Adsorbent

The cellulose–hydroxyapatite was blended with the graphene-modified activated carbon, crosslinked using citric acid (1 g), and dried at 80 °C to obtain the final hybrid adsorbent.

Step 6: Preparation of Carbon Cloth (Comparative Study)

Cotton fabric was carbonized at 500 °C for 2 h to obtain carbon cloth, dip-coated in graphene oxide suspension (1 mg mL^{-1}), reduced using plant extract, and alternately immersed in 0.3 M $CaCl_2$ and 0.2 M KH_2PO_4 solutions to deposit hydroxyapatite layers.

Step 7: Synthesis of Magnetic

Magnetic Fe_3O_4 nanoparticles were synthesized via a green co-precipitation method using $FeCl_3 \cdot 6H_2O$ (2.7 g) **and** $FeSO_4 \cdot 7H_2O$ (1.4 g) as iron precursors in an alkaline medium (pH ≈ 10), with plant extract serving as the reducing and stabilizing agent. The synthesized Fe_3O_4 nanoparticles were subsequently incorporated into the carbon–graphene matrix, followed by the **in situ** deposition of hydroxyapatite to obtain the final composite material.

Step 8: Batch Adsorption Experiments

Batch adsorption studies were carried out by adding 0.1 g of adsorbent to 100 mL fluoride solution (10 mg L^{-1}) under agitation at 150 rpm. After adsorption, the adsorbents were separated by filtration or magnetic decantation, and residual fluoride concentration was determined using standard analytical methods.

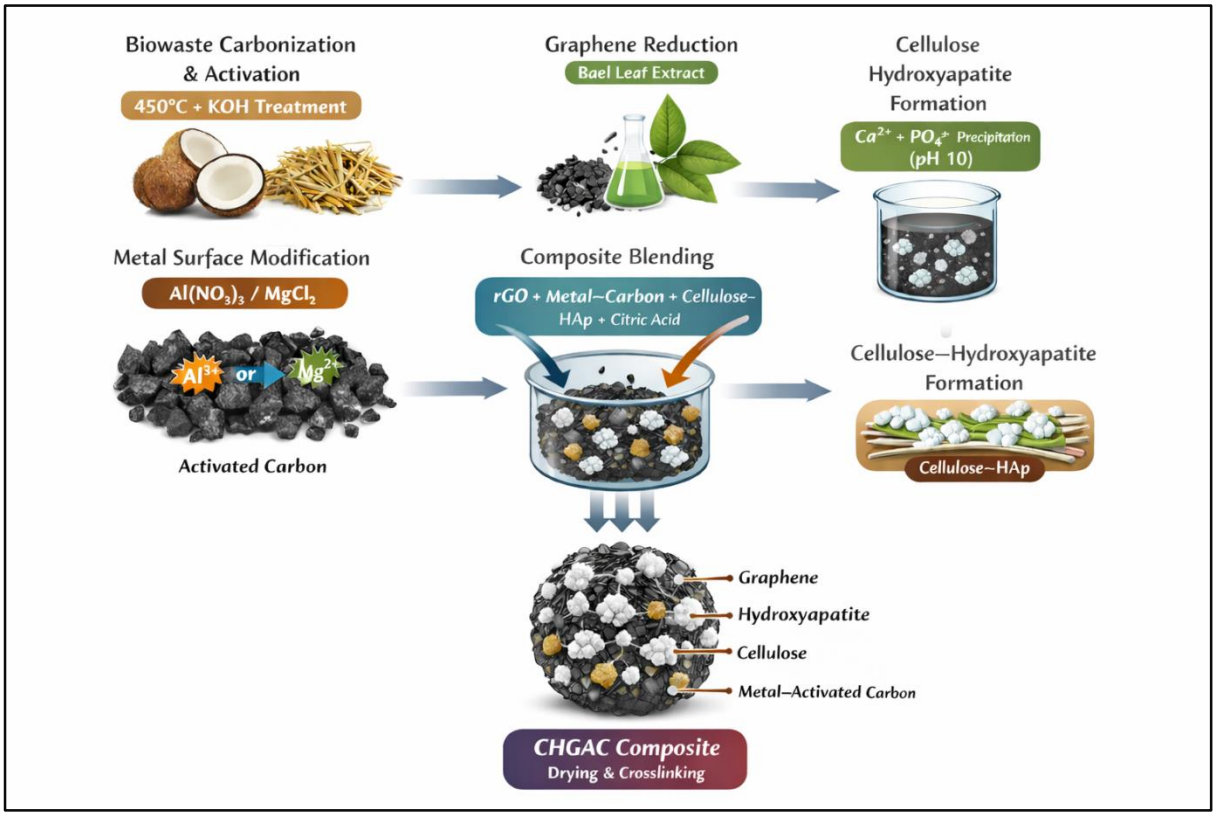

Figure 7: Diagrammatic representation of the synthesis procedure of the composite

Conclusion:

The CHGAC (Cellulose–Hydroxyapatite–Graphene Activated Carbon) was successfully synthesized and thoroughly characterized using XRD, FTIR, and TGA, confirming its crystalline structure, presence of functional groups responsible for fluoride adsorption, and high thermal stability. Water samples from the Dungarpur region, including wells, boreholes, hand pumps, and municipal taps, were tested to evaluate the's practical performance. The CHGAC exhibited high initial fluoride removal efficiency (~95%) and maintained substantial adsorption capacity over multiple adsorption–desorption cycles**,** demonstrating its excellent recyclability. This indicates that the active sites of the remain largely intact even after repeated use. The study shows that the CHGAC combines structural robustness, functional versatility, and sustained adsorption performance**,** making it an effective and practical solution for mitigating fluoride contamination in groundwater. Its consistent performance across different water sources and repeated cycles highlights its potential as a sustainable and reusable adsorbent**,** offering a reliable approach for providing safe drinking water to fluoride-affected communities.

Acknowledgment:

The authors gratefully acknowledge the Department of Chemistry, Mohanlal Sukhadia University, Udaipur, for providing the necessary infrastructure for characterization work. They also extend their sincere thanks to SAIF, Chandigarh, and IIT Jammu for their support in carrying out advanced characterization analyses.

Conflict of Interest:

The author declares no conflict of interest.

References:

1) Ali, S., Thakur, S. K., Sarkar, A., & Shekhar, S. (2016). Worldwide contamination of water by fluoride. *Environmental chemistry letters*, *14*(3), 291-315.

2) Ahmad, S., Singh, R., Arfin, T., & Neeti, K. (2022). Fluoride contamination, consequences and removal techniques in water: a review. *Environmental Science: Advances*, *1*(5), 620-661.

3) Bibi, S., Kamran, M. A., Sultana, J., & Farooqi, A. (2017). Occurrence and methods to remove arsenic and fluoride contamination in water. *Environmental chemistry letters*, *15*(1), 125-149.

4) Sankhla, M. S., & Kumar, R. (2018). Fluoride contamination of water in India and its impact on public health. *ARC Journal of Forensic Science*, *3*(2), 10-15.

5) Roy, S., & Dass, G. (2013). Fluoride contamination in drinking water–a review. *Resour. Environ*, *3*(3), 53-58.

6) Thole, B. (2013). Ground water contamination with fluoride and potential fluoride removal technologies for East and Southern Africa. In *Perspectives in water pollution*. IntechOpen.

7) Ayoob, S., Gupta, A. K., & Bhat, V. T. (2008). A conceptual overview on sustainable technologies for the defluoridation of drinking water. *Critical reviews in environmental science and technology*, *38*(6), 401-470.

8) Mumtaz, N., Pandey, G., & Labhasetwar, P. K. (2015). Global fluoride occurrence, available technologies for fluoride removal, and electrolytic defluoridation: a review. *Critical Reviews in Environmental Science and Technology*, *45*(21), 2357-2389.

9) Mousazadeh, M., Alizadeh, S. M., Frontistis, Z., Kabdaşlı, I., Karamati Niaragh, E., Al Qodah, Z., ... & Emamjomeh, M. M. (2021). Electrocoagulation as a promising defluoridation technology from water: a review of state of the art of removal mechanisms and performance trends. *Water*, *13*(5), 656.

10) Shrivastava, B. K., & Vani, A. (2009). Comparative study of defluoridation technologies in India. *Asian J. Exp. Sci*, *23*(1), 269-274.

11) Agarwal, K. C., Gupta, S. K., & Gupta, A. B. (1999). Development of new low cost defluoridation technology (KRASS). *Water science and technology*, *40*(2), 167-173.

12) Patra, B. R., Mukherjee, A., Nanda, S., & Dalai, A. K. (2021). Biochar production, activation and adsorptive applications: a review. *Environmental Chemistry Letters*, *19*(3), 2237-2259.

13) Panwar, N. L., & Pawar, A. (2022). Influence of activation conditions on the physicochemical properties of activated biochar: a review. *Biomass Conversion and Biorefinery*, *12*(3), 925-947.

14) Ku, Y., & Chiou, H. M. (2002). The adsorption of fluoride ion from aqueous solution by activated alumina. *Water, air, and soil pollution*, *133*(1), 349-361.

15) George, S., Pandit, P., & Gupta, A. B. (2010). Residual aluminium in water defluoridated using activated alumina adsorption–modeling and simulation studies. *water research*, *44*(10), 3055-3064.

16) Ku, Y., & Chiou, H. M. (2002). The adsorption of fluoride ion from aqueous solution by activated alumina. *Water, air, and soil pollution*, *133*(1), 349-361.

17) Pu'ad, N. M., Haq, R. A., Noh, H. M., Abdullah, H. Z., Idris, M. I., & Lee, T. C. (2020). Synthesis method of hydroxyapatite: A review. *Materials Today: Proceedings*, *29*, 233-239.

18) Nayak, B., Samant, A., Patel, R., & Misra, P. K. (2017). Comprehensive understanding of the kinetics and mechanism of fluoride removal over a potent nanocrystalline hydroxyapatite surface. *ACS omega*, *2*(11), 8118-8128.

19) Zhang, J., Chen, N., Su, P., Li, M., & Feng, C. (2017). Fluoride removal from aqueous solution by zirconium-chitosan/graphene oxide membrane. *Reactive and Functional Polymers*, *114*, 127-135.

20) Xu, N., Li, S., Li, W., & Liu, Z. (2020). Removal of fluoride by graphene oxide/alumina nanocomposite: Adsorbent preparation, characterization, adsorption performance and mechanisms. *ChemistrySelect*, *5*(6), 1818-1828.

21) Park, G., Hong, S. P., Lee, C., Lee, J., & Yoon, J. (2021). Selective fluoride removal in capacitive deionization by reduced graphene oxide/hydroxyapatite composite electrode. *Journal of Colloid and Interface Science*, *581*, 396-402.

22) Sun, R., Zhang, H. B., Qu, J., Yao, H., Yao, J., & Yu, Z. Z. (2016). Supercritical carbon dioxide fluid assisted synthesis of hierarchical AlOOH@ reduced graphene oxide hybrids for efficient removal of fluoride ions. *Chemical Engineering Journal*, *292*, 174-182.